Ore Geology Reviews 44 (2012) 1–9

Contents lists available at SciVerse ScienceDirect

Ore Geology Reviews

journal homepage: www.elsevier.com/locate/oregeorev

Review

The application of ASTER remote sensing data to porphyry copper and epithermal gold deposits

Amin Beiranvand Pour, Mazlan Hashim *

Institute of Geospatial Science & Technology (INSTeG), Universiti Teknologi Malaysia, 81310 UTM Skudai, Johor Bahru, Malaysia

ARTICLE INFO

Article history:
Received 18 September 2010
Received in revised form 26 July 2011
Accepted 14 September 2011
Available online 17 September 2011

Keywords:
ASTER
Copper/gold exploration
Porphyry
Alteration zones
ASTER standard data products
Logical operator algorithms

ABSTRACT

This paper reviews the performance characteristics of the Advanced Spaceborne Thermal Emission and Reflection Radiometer (ASTER) remote sensor, the standard data products, and applications of the most recently developed image processing methods applied to ASTER data as a tool for mapping hydrothermal alteration mineral zones associated with porphyry copper and epithermal gold mineralization and related host-rock lithology. Hydrothermal alteration zones associated with porphyry copper deposit such as phyllic, argillic, and propylitic mineral assemblages can be discriminated from one another by virtue of their spectral absorption features, which are detectable by ASTER SWIR spectral bands. The identification of the phyllic zone is important in the initial stages of porphyry copper exploration as an indicator of high economic-potential for copper mineralization.

Two new crosstalk-corrected ASTER SWIR reflectance products including AST-07XT and RefL1b are more reliable than previous ASTER data products for regional mineral mapping without use of additional spectral data from the site for calibration. Four types of algorithms were used to extract spectral information of ASTER data: 1) band-ratio, indices and logical operator based methods; 2) principal components and enhancement based methods such as Principal Component Analysis (PCA) and Minimum Noise Fraction (MNF); 3) shape-fitting based algorithms such as Spectral Angle Mapper (SAM), Matched-Filtering (MF), and Mixture-Tuned Matched-Filtering (MTMF); and 4) partial unmixing methods such as Linear Spectral Unmixing (LSU) and Constrained Energy Minimization (CEM).

This review emphasizes that the logical operator algorithms can be best suited for hydrothermal alteration mineral mapping, including phyllic and argillic zones associated with porphyry copper mineralization in a regional scale. Shape-fitting based and partial unmixing algorithms are robust and reliable for detecting particular mineral and mineral assemblages in hydrothermal alteration zones in a district scale. Consequently, the integration of the results derived from the logical operator, shape-fitting based, and partial unmixing algorithms can produce comprehensive and accurate information for the reconnaissance stages of copper and gold exploration at both regional and district scales. All of the methods and applications reviewed in this paper demonstrate the utility of ASTER data for exploration of the porphyry copper and epithermal gold deposits around the world.

Contents

* Corresponding author. Tel.: +60 7 5530666; fax: +60 7 5531174.
E-mail addresses: mazlanhashim@utm.my, profmhashim@gmail.com (M. Hashim).

0169-1368/$ – see front matter © 2011 Elsevier B.V. All rights reserved.
doi:10.1016/j.oregeorev.2011.09.009

1. Introduction

Porphyry copper deposits are generated by hydrothermal fluid processes that alter the mineralogy and chemical composition of the country rocks (e.g., Ferrier and Wadge, 1996; Ferrier et al., 2002; Hunt and Ashley, 1979). Alteration produces distinctive mineral assemblages with diagnostic spectral absorption features in the visible and near infrared (VNIR) through the shortwave length infrared (SWIR) (0.4–2.5 μm) and/or the thermal infrared (TIR) (8.0–14.0 μm) wavelength regions (Abrams and Brown, 1984; Abrams et al., 1983; Spatz and Wilson, 1995).

Porphyry copper deposits typically occur in association with hydrothermal alteration mineral zones such as phyllic, argillic, potassic, and propylitic (Fig. 1; Lowell and Guilbert, 1970). A core of quartz and potassium-bearing minerals is surrounded by multiple zones that contain clay and other hydroxyl-bearing minerals with diagnostic spectral absorption properties in the visible and near infrared through the shortwave length infrared portions of the electromagnetic spectrum.

Supergene alteration processes over porphyry copper bodies produce an oxide zone with extensive iron oxide/hydroxide minerals (yellowish to reddish color altered rocks), which are collectively termed gossan (Abdelsalam and Stern, 2000; Sabins, 1999). Iron oxide/hydroxide minerals such as limonite, jarosite, and hematite tend to have low reflectance in visible and higher reflectance in near infrared wavelength region (Hunt, 1977; Hunt and Salisbury, 1974). Electronic processes produce absorption features in the visible and near infrared radiation (0.4 to 1.1 μm) due to the presence of transition elements such as Fe^{2+}, Fe^{3+} and often substituted by Mn, Cr, and Ni in the crystal structure of the minerals (Hunt, 1977; Hunt and Ashley, 1979).

Hydroxyl-bearing minerals, including clay and sulfate groups, as well as carbonate minerals present diagnostic spectral absorption features due to vibrational processes of fundamental absorptions of Al–O–H, Mg–O–H, Si–O–H, and CO_3 groups in the shortwave length infrared region of the electromagnetic spectrum (Clark et al., 1990; Crowley and Vergo, 1988; Hunt, 1977; Hunt and Ashley, 1979). Hence, shortwave length infrared data can be used for the identification of hydrothermal alteration mineral assemblages including: (i) mineralogy generated by the passage of low-pH fluids (alunite and pyrophylite); (ii) Al–Si-(OH) and Mg–Si-(OH)-bearing minerals, including kaolinite and mica and cholorite groups; and (iii) Ca–Al–Si-(OH) bearing minerals such as epidote group, as well as carbonate group (calcite and dolomite) (Huntington, 1996).

Hydrothermal alteration minerals with diagnostic spectral absorption properties in the visible and near infrared through the shortwave length infrared regions can be identified by multispectral and hyperspectral remote sensing data as a tool for the initial stages of porphyry copper and epithermal gold exploration (Bedini et al., 2009; Carranza and Hall, 2002; Di Tommaso and Rubinstein, 2007; Gabr et al., 2010; Kruse et al., 2003; Mars and Rowan, 2006; Moore et al., 2008; Perry, 2004; Pour et al., 2011; Tangestani and Moore, 2002; Tangestani et al., 2008; Yujun et al., 2007; Zhang et al., 2007). Porphyry copper deposits presently provide nearly three-quarters of world's Cu, half the world's Mo, perhaps one-fifth of the world's Au, most of the world's Re, and minor amount of other metals such as Ag, Pd, Te, Se, Bi, Zn, and Pb (Sillitoe, 2010). The differentiation between the three hydrothermal alteration zones and especially targeted identification of the phyllic zone are important in the exploration of porphyry copper mineralization, because phyllic zone is an indicator of high-economic potential for copper mineralization within the central shell of mineralization as shown in Fig. 1. This alteration zone normally overprints potassic and chlorite–sericite alteration assemblages (Dilles and Einaudi, 1992; Sillitoe, 2010).

The Advanced Spaceborne Thermal Emission and Reflection Radiometer (ASTER) remote sensor has sufficient spectral resolution in the shortwave length infrared radiation bands for mapping hydrothermal alteration mineral zones associated with porphyry copper and epithermal gold mineralization. Fig. 2 shows the wavelength locations of ASTER spectral bands across the electromagnetic spectrum (after Pieri and Abrams, 2004).

Ideal porphyry copper deposits are typically characterized by hydrothermal alteration mineral zones (Fig. 1; Lowell and Guilbert, 1970), of which the core of quartz and potassium-bearing minerals is surrounded by multiple zones. The broad phyllic zone is characterized by illite/muscovite (sericite) which yields an intense Al-OH absorption feature centered at 2.20 μm, coinciding with ASTER band 6. The narrower argillic zone includes kaolinite and alunite, which collectively displays a secondary Al-OH absorption feature at 2.17 μm that corresponds with ASTER band 5. The mineral assemblages of the outer propylitic zone include epidote, chlorite, and calcite which all exhibit absorption features situated at 2.35 μm, which coincide with ASTER band 8 (Fig. 3) (Clark et al., 1990; Crowley and Vergo, 1988; Dalton et al., 2004; Hunt, 1977; Hunt and Ashley, 1979; Mars and Rowan, 2006; Rowan et al., 2006; Spatz and Wilson, 1995).

Since 2000, ASTER data have been widely and successfully used in lithological mapping and mineral exploration. Accordingly, this paper reviews the performance characteristics of ASTER sensor, ASTER standard data products, and applications of the most recently developed image processing methods applied to ASTER data as a tool for mapping hydrothermal alteration mineral zones associated with porphyry copper and epithermal gold mineralization and related host-rock lithology.

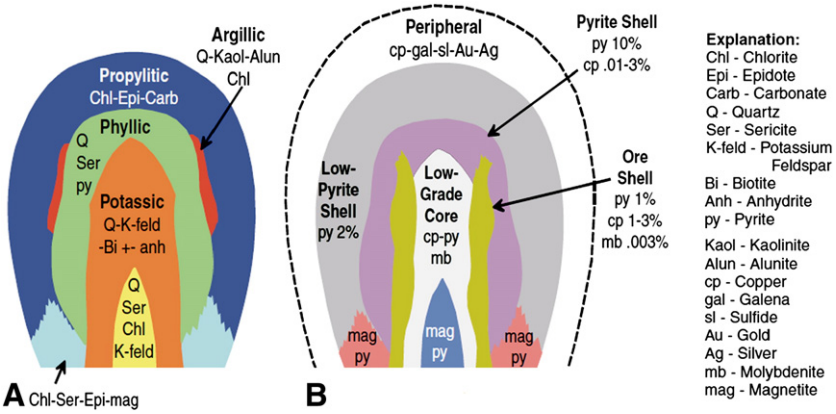

Fig. 1. Hydrothermal alteration zones associated with porphyry copper deposit, modified from Lowell and Guilbert (1970), and Mars and Rowan (2006). (A) Schematic cross section of hydrothermal alteration mineral zones, which consist of propylitic, phyllic, argillic, and potassic alteration zones. (B) Schematic cross section of ores associated with each alteration zone.

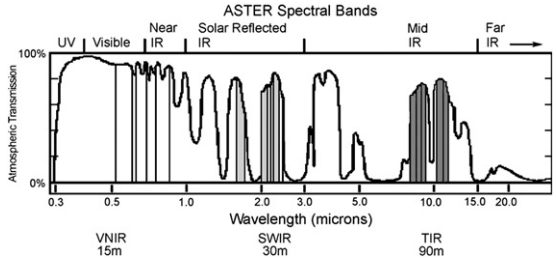

Fig. 2. ASTER spectral bands in the wavelength of the electromagnetic spectrum (after Pieri and Abrams, 2004).

2. Advanced Spaceborne Thermal Emission and Reflection Radiometer data

The Advanced Spaceborne Thermal Emission and Reflection Radiometer (ASTER) is a high spatial, spectral, and radiometric resolution multispectral remote sensing instrument. It was launched on NASA's Earth Observing System AM-1 (EOS AM-1) polar orbiting spacecraft, Terra in December 1999. EOS AM-1 spacecraft operates in a near polar, sun-synchronous orbit at 705 km altitude in a circular. The recurrent cycle is 16 days, with additional 4 day repeat coverage due to its off-nadir pointing capabilities. ASTER is a cooperative effort between the Japanese Ministry of Economic Trade and Industry (METI) and National Aeronautics and Space Administration (NASA). It consists of three separate instrument subsystems, which provide observation in three different spectral regions of the electromagnetic spectrum, including visible and near infrared (VNIR), shortwave length infrared (SWIR) and thermal infrared (TIR). The VNIR subsystem has three recording channels between 0.52 and 0.86 μm and an additional backward-looking band for stereo construct of Digital Elevation Models (DEMs) with a spatial resolution of up to 15 m. The SWIR subsystem has six recording channels from 1.6 to 2.43 μm, at a spatial resolution of 30 m, while the TIR subsystem has five recording channels, covering the 8.125 to 11.65 μm wavelength region with spatial resolution of 90 m. ASTER swath width is 60 km (each individual scene is cut to a 60×60 km^2 area), which makes it useful for regional mapping, though its off-nadir pointing capability extends its total possible field of view to up to 232 km. ASTER can acquire approximately 600 scenes daily, but is generally targeted and tasked without continuous operation unlike other multispectral sensors such as Landsat (Abrams, 2000; Abrams and Hook, 1995; Abrams et al., 2004; Fujisada, 1995; Yamaguchi et al., 1999; Yamaguchi et al., 2001).

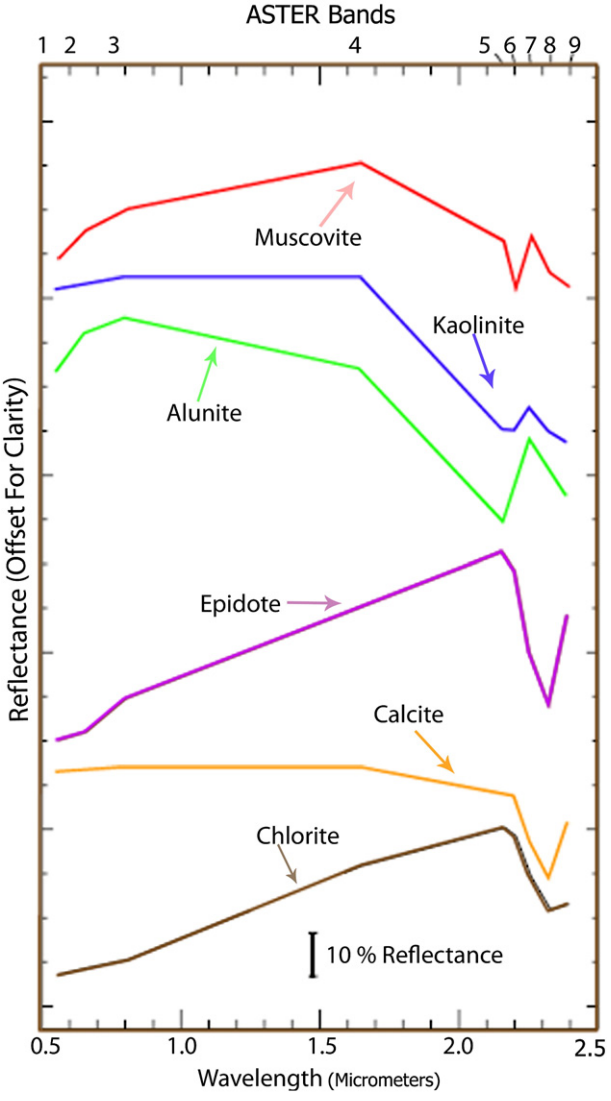

Fig. 3. Laboratory spectra of muscovite, kaolinite, alunite, epidote, calcite, and chlorite resampled to ASTER bandpasses. Spectra include muscovite, which is typical in phyllic alteration zone, with a 2.20 μm absorption feature; kaolinite and alunite, which are common in argillic alteration zone, have 2.17 μm secondary absorption features; and epidote, calcite, and chlorite, which are typically associated with propylitic alteration zone and display 2.35 μm absorption features (Clark et al., 1993; modified from Mars and Rowan, 2006).

ASTER provides data useful for studying the interaction among the geosphere, hydrosphere, cryosphere, lithosphere, and atmosphere of the earth from an earth system science perspective. To be more specific, wide range of science investigations and applications include: (a) geology and soil studies; (b) land surface climatology studies; (c) vegetation and ecosystem dynamic studies; (d) volcano monitoring; (e) other natural hazard monitoring; (f) carbon cycle and marine ecosystem studies; (g) hydrology and water resource applications; (h) aerosol and cloud studies; (i) seasonal evapotranspiration measurements; and (j) land surface and land cover change analyses (Fujisada, 1995; Gillespie et al., 2005).

Significant from the standpoint of geologic mapping applications are: (1) ASTER is the first multispectral spaceborne sensor that allows the discrimination and identification of hydrothermal alteration minerals in the shortwave infrared (SWIR) region of the electromagnetic spectrum (Abrams and Hook, 1995); (2) ASTER visible and near infrared (VNIR) and thermal infrared (TIR) data can provide sufficient capability for the remote identification of vegetation and iron oxide minerals in surface soil and the mapping of carbonates and silicates, respectively (Bedell, 2001; Ninomiya, 2003a; Rockwell and Hofstra, 2008).

ASTER standard data products are available 'on-demand' from the Earth Remote Sensing Data Analysis Center (ERSDAC; Japan) and the EROS data center (EDC; USA). Basically, all of the ASTER captured data are processed to generate Level-1A data product, which consists of unprocessed raw image data and coefficients for radiometric correction. The Level-1B (radiance-at-sensor) data product is a re-sampled image data generated from the Level-1A data by applying the radiometric and geometric correction coefficients (Abrams et al., 2004). Level-2 data products of measured physical parameters include: surface radiance data with nominal atmospheric corrections (Level-2B01), surface reflectance data contains atmospherically corrected VNIR-SWIR data (Level-2B07 or AST-07), surface emissivity data with MODTRAN atmospheric correction and a temperature-emissivity separation (TES) algorithm (Level-2B04), which are all generated based on user request (Gillespie et al., 1998; Thome et al., 1998; Yamaguchi et al., 1999).

Level-4B data product is also generated under the user request from the along-track stereo observation in the near infrared channel (band 3N and 3B) in order to construct Digital Elevation Models (DEMs). Level-3A is a geometrically well-corrected orthorectified ASTER standard data product with ASTER-driven DEM, which is radiometrically

equivalent to Level-1B radiance-at-sensor data (Abrams, 2000; Ninomiya, 2003a, b, c; Ninomiya et al., 2005; Yamaguchi et al., 2001).

During scene acquisition of ASTER data, there is optical 'crosstalk' effect caused by stray of light from band 4 detector into adjacent band 5 and 9 detectors on SWIR subsystem (Iwasaki and Tonooka, 2005). Such deviations from correct reflectance result in false absorption features and distortion of diagnostic signatures which result in spectroscopic misidentification of minerals (Mars and Rowan, 2010). Fortunately, ASTER Cross-Talk correction software is available from www.gds.aster.ersdac.or.jp (Hewson et al., 2005; Iwasaki and Tonooka, 2005; Kanlinowski and Oliver, 2004).

Recently, two new crosstalk-corrected ASTER SWIR reflectance products had been released, which include: (1) AST-07XT SWIR reflectance data product available 'on-demand' from ERSDAC and EDC (Iwasaki and Tonooka, 2005), and (2) RefL1b SWIR reflectance data product generated and described by Mars and Rowan (2010). The AST-07XT SWIR surface reflectance data product is similar to AST-07 surface reflectance data in that it consists of the same VNIR and SWIR bands. However, the crosstalk correction algorithm and atmospheric correction (non-concurrently acquired MODIS water vapor data) has been pre-applied to the data (Biggar et al., 2005; Iwasaki and Tonooka, 2005; Mars and Rowan, 2010). RefL1b and AST-07XT reflectance datasets both attempt to correct for the SWIR anomaly. However, the differences between these datasets are caused by the addition of the radiometric correction factors and use of concurrently acquired water vapor data for atmospheric correction in the case of the RefL1b data. Spectral analyst results for AST-07XT and RefL1b indicated that these new ASTER products can be used for regional mineral mapping without use of additional spectral data from the site for calibration. Especially, ASTER mineral mapping projects will be more feasible using RefL1b data (Mars and Rowan, 2010).

3. Mapping mineralization-related hydrothermal alteration mineral zones using ASTER data

In this section, we review applications of the most recently developed image processing methods applied to ASTER data as a tool for mapping hydrothermal alteration mineral zones associated with porphyry copper and epithermal gold mineralization and related host-rock lithology.

Rowan et al. (2003) evaluated the capability of the ASTER data for mapping the hydrothermally altered rocks and the unaltered country rocks in the Cuprite mining district in Nevada, USA. They used Matched-Filtering (MF; Harsanyi et al., 1994) for identifying the surface distribution of hydrothermal alteration minerals. Their results indicated that spectral reflectance differences in the nine bands of visible and near infrared through the shortwave infrared (0.52 to 2.43 μm) can provide subtle spectral information for discriminating the main hydrothermal alteration mineral zones depicted in Fig. 1. For example, they identified a silicified zone, an opalized zone, an argillized zone and the distribution of unaltered country rock units. Their results compared well with those obtained using Airborne Visible/Infrared Imaging Spectrometer (AVIRIS) hyperspectral data.

Yamaguchi and Naito (2003) proposed several spectral indices for lithological discrimination and mapping of exposed surface rock types using ASTER shortwave length infrared (SWIR) bands. For example, Alunite Index, Kaolinite Index, Calcite Index, and Montmorillonite Index were calculated using linear combinations of reflectance values in each of the six SWIR bands.

Because ASTER has 14 spectral bands, many permutations of ratio images, and thus more lithologic and mineralogic indices (including complex logical operators such as those used by Mars and Rowan, 2006) can be derived from ASTER data. For example, Ninomiya (2003a, 2003b) defined a vegetation index and mineralogic indices for ASTER VNIR and SWIR bands, as well as lithologic indices for ASTER TIR bands by considering the spectral absorption features of vegetation and different minerals and rocks in ASTER spectral channels. The resulting indices are listed as follows:

$$\text{Stabilized Vegetation Index (StVI)} = \left[\frac{band3}{band2}\right]\left[\frac{band1}{band2}\right] \quad (1)$$

$$\text{OH bearing altered minerals Index(OHI)} = \left[\frac{band7}{band6}\right]\left[\frac{band4}{band6}\right] \quad (2)$$

$$\text{Kaolinite Index (KLI)} = \left[\frac{band4}{band5}\right]\left[\frac{band8}{band6}\right] \quad (3)$$

$$\text{Alunite Index (ALI)} = \left[\frac{band7}{band5}\right]\left[\frac{band7}{band8}\right] \quad (4)$$

$$\text{Calcite Index (CLI)} = \left[\frac{band6}{band8}\right]\left[\frac{band9}{band8}\right] \quad (5)$$

$$\text{Quartz Index (QI)} = \frac{(band11 * band11)}{band10 * band12} \quad (6)$$

$$\text{Carbonate Index (CI)} = \frac{band13}{band14} \quad (7)$$

$$\text{Mafic Index (MI)} = \frac{band12}{band13} \quad (8)$$

These spectral indices have been applied to ASTER Level-1B radiance at the sensor data covering the Cuprite district, Nevada in USA; Yarlung Zangbo ophiolite zone in Tibet; Beishan Mountains area in China; North-western Gansu province in China; and an ophiolite zone in Oman (Ninomiya, 2003c, 2004; Ninomiya and Fu, 2002). These indices provided accurate spectral information for vegetation, minerals, and lithological mapping, while showing the spatial distribution of these materials well. Also, the resulting maps yielded excellent spatial coherency and strong correlations to published geologic maps of the study areas.

Crosta et al. (2003) used Principal Component Analysis (PCA) on ASTER VNIR and SWIR bands in order to target key alteration minerals associated with epithermal gold deposits in Los Menucos, Patagonia, Argentina. PCA was applied to selected subsets of four ASTER bands according to the position of characteristic spectral absorption features of key hydrothermal alteration mineral end-members such as alunite, illite, smectite, and kaolinite in the VNIR and SWIR regions. Their results revealed that PCA technique can extract detailed mineralogical spectral information from ASTER data by producing abundance images of selected minerals. Thus, this technique can be used for identifying hydrothermal alteration minerals associated with precious and base-metal deposits.

Velosky et al. (2003) distinguished the propylitic alteration zone and gossan associated with massive sulfide mineralization in host rocks by using ASTER (4/2, 4/5, 5/6) band ratio images covering the Neoproterozoic Wadi Bidah shear zone, southwestern Saudi Arabia. Xu et al. (2004) identified hydrothermal alteration mineral zones around epithermal gold deposits using ASTER data in the northeastern part of Laizhou region, China. They used PCA technique and band ratio of 3/2, 4/1, and 4/6 for delimitating of vegetation, iron oxide, and clay minerals, respectively.

Hewson et al. (2005) generated "seamless" regional-scale maps of Al-OH and Mg-OH/carbonate minerals and ferrous iron content from ASTER SWIR data, as well as a map of quartz content from ASTER TIR data for the Broken Hill–Curnamona province of Australia. Rowan et al. (2005) evaluated ASTER band ratios and Relative absorption Band Depth images (RBD —Crowley et al., 1989), Matched-Filtering (MF —Harsanyi et al., 1994) and Spectral Angle Mapper (SAM — Kruse et al., 1993) methods for lithological mapping of the ultramafic complex of Mordor Pound, NT, Australia. They identified subtle and

major spectral features useful for distinguishing and classifying felsic and mafic–ultramafic rocks, alluvial–colluvial deposits and quartzose to intermediate composition rocks from one another. Their classification results were based on spectral absorption features of Al-OH and ferric-iron mineralogical groups for felsic rocks; and ferrous-iron and Fe,Mg-OH mineralogical absorption features for mafic–ultramafic rocks using the VNIR + SWIR bands of ASTER. Additional Si–O spectral features were used to map more lithologic diversity within ultramafic and adjacent rocks such as mafic–gneisses, felsic–gneisses, intermediate composition rocks such as syenite, and quartzite using ASTER TIR data.

Galvao et al. (2005) used the Spectral Angle Mapper (SAM) method on ASTER SWIR bands to investigate spectral discrimination of hydrothermally altered minerals in a tropical savannah environment, in the northern portion of Gious state, central Brazil. Their results showed the efficacy of ASTER SWIR data in discriminating areas of altered minerals from the surrounding vegetated environment.

Rowan et al. (2006) identified the distribution of hydrothermally altered rocks consisting of phyllic, argillic and propylitic alteration zones based on spectral analysis of VNIR + SWIR ASTER bands. Additional hydrothermally silicified rocks were mapped using TIR ASTER bands covering the Reko Diq, Pakistan Cu–Au mineralized area.

In a follow up study, Mars and Rowan (2006) developed logical operator algorithms based on ASTER defined band ratios for regional mapping of phyllic and argillic altered rocks in the Zargros magmatic arc, Iran. The logical operator algorithms were used to illustrate distinctive patterns of argillic and phyllic alteration zones associated with Eocene to Miocene intrusive igneous rocks, as well as known and undiscovered porphyry copper deposits. Numerous high-potential areas of porphyry copper and epithermal or polymetallic vein-type mineralization were identified based on argillic and phyllic alteration patterns in the study area.

Ducart et al. (2006) applied Mixture-Tuned Matched-Filtering (MTMF —Boardman et al., 1995) method to ASTER SWIR data to provide regional and local information on the spatial distribution of hydrothermal alteration zones associated with epithermal gold mineralization at the Somún Curá Massif, Patagonia, Argentina. Three major areas of alteration were clearly recognized: Cerro La Mina, Cerro Abanico, and Aguada de Guerra. They identified alteration zones such as advanced argillic, argillic, and silicic with satisfactory correlation with their field spectroscopy data.

Di Tommaso and Rubinstein (2007) used band ratios, certain color band combinations, and the Spectral Angle Mapper (SAM) method for mapping hydrothermal alteration minerals associated with Infiernillo porphyry copper deposit using ASTER data covering the San Rafale Massif, southern Mendoza Province, Argentina. They detected illite, kaolinite, sericite and jarosite through spectral analysis of SWIR bands, and surface silica and potassic alteration using ASTER TIR bands. Yujun et al. (2007) delineated hydrothermal alteration anomalies for predicting Cu–Au mineral resources using ASTER data covering Oyu Tolgoi, Mongolian, the Spectral Angle Mapper (SAM) algorithm and Principal Component Analysis (PCA).

Zhang et al. (2007) evaluated ASTER surface reflectance (AST-07) data for gold-hosted lithologic mapping and alteration mineral detection in the south Chocolate Mountains area, California, USA. They applied PCA transformation to mineralogic indices, including the OH bearing altered mineral Index (OHI), Kaolinite Index (KLI), Alunite Index (ALI), and Calcite Index (CLI) for delineating alteration zones. The Constrained Energy Minimization (CEM) technique (a subpixel linear spectral unmixing-LSU algorithm —Farrand and Harsanyi, 1994) was used to detect alunite, kaolinite, muscovite, and montmorillonite fractional abundances using ASTER VNIR and SWIR surface reflectance data and reference spectra from the ASTER spectral library (Baldridge et al., 2009).

Moghtaderi et al. (2007) used ASTER data for distinguishing sodic–calcic, potassic, and silicic–phyllic alteration patterns associated with hydrothermal iron oxide features across the Chadormalu paleocrater, Bafq region, Central Iran. The alteration minerals were identified by using False Color Composite (FCC) images, Decorrelation-stretch images, and Minimum Noise Fraction (MNF) images.

Rockwell and Hofstra (2008) used ASTER thermal infrared emissivity data for identifying quartz and carbonate minerals in northern Nevada, USA. A Quartz Index (QI) and a Carbonate Index (CI) were implemented using ASTER Level 2 surface emissivity (Level-2B04) data for geologic mapping and mineral resource investigation purposes. They concluded that mapping hydrothermal quartz and carbonate rocks at regional and local scales have considerable economical attention for ore deposit exploration, because these rocks can be host rock a wide range of metallic ore deposit types.

Tangestani et al. (2008) evaluated ASTER Level-1B 'radiance-at-sensor' and surface reflectance (AST-07) data for alteration zone enhancement related to porphyry copper mineralization in northern Shahr-e-Babak, Iran. Directed Principal Component Analysis (DPCA) and Spectral Angle Mapper (SAM) methods were used to map pixels containing illite, chlorite, and muscovite minerals. Moore et al. (2008) mapped mineral alteration associated with gold deposits using ASTER Level 1A data in the Takab area, north-west Iran. They applied selective band principal component analysis, Relative absorption Band-Depth (RBD), and Matched-Filtering (MF) methods for discriminating between argillic and silicic alteration types.

Kratt et al. (2010) analyzed ASTER VNIR and SWIR band combinations using a decorrelation stretch algorithm for identifying areas containing hydrothermally altered rocks and tufa deposition at Pyramid Lake, Nevada, USA. Gabr et al. (2010) detected areas of high-potential gold mineralization using ASTER surface reflectance (AST-07) data covering Abu-Marawat, North-Eastern Desert of Egypt. Spectral discrimination between high-potential and low-potential areas of gold mineralization was recognized by utilizing PCA transformed mineral indices, color ratio images (e.g., 4/8, 4/2, 8/9 displayed as RGB), Constrained Energy Minimization (CEM) and Spectral Angle Mapper (SAM) methods. The results of their field investigations proved the accuracy of their image processing results.

Mars and Rowan (2010) assessed two new ASTER SWIR surface reflectance data products, namely RefL1b and AST-07XT for spectroscopic mapping of rocks and minerals. Their results indicated that the new ASTER products are more reliable than previous ASTER products for discriminating hydrothermal alteration minerals and mineral groups without use of additional spectral data from the site for calibration.

Pour et al. (2011) discriminated hydrothermal alteration zones associated with Meiduk and Sar Cheshmeh porphyry copper deposits using ASTER Level-1B 'radiance-at-sensor' data in the Urumieh-Dokhtar volcanic belt, southeastern Iran. They applied shape-fitting based and partial unmixing algorithms, including Spectral Angle Mapper (SAM), Linear Spectral Unmixing (LSU), Matched-Filtering (MF), and Mixture-Tuned Matched-Filtering (MTMF) to shortwave infrared length radiation bands of ASTER. These methods discriminated the phyllic, argillic, and propylitic alteration zones, as well as highlighting the phyllic zone as indicator of high-economic potential area for copper mineralization. Pour and Hashim (2011) investigated spectral transformation of ASTER bands using Principal Component Analysis (PCA), Minimum Noise Fraction (MNF), and band ratio methods for two major copper mining districts (Meiduk and Sar Cheshmeh) in the Urumieh-Dokhtar volcanic belt, southeastern Iran. PCA images detected vegetation and iron oxide minerals using the VNIR bands. Clay minerals and silicate-rich rocks were identified using SWIR and TIR PCA images, respectively. Their PCA results have been verified by minimum noise fraction and band ratio methods, as well as prior knowledge about the study areas.

As the literature admits, there are four types of algorithms that can be applied to ASTER data to map, enhance, and discriminate hydrothermal alteration mineral types associated with porphyry copper and epithermal gold mineralization as follows. 1) Band-ratio, indices and logical operator based methods (Crowley et al., 1989; Goetz et al., 1983; Mars and Rowan, 2006; Ninomiya,

2003a, 2003b; Rowan et al., 1977; Sabins, 1987); 2) principal components and enhancement/display based methods such as Principal Component Analysis (PCA) (Singh and Harrison, 1985) and Minimum Noise Fraction (MNF) (Boardman et al., 1995; Green et al., 1988), or simple color display of key bands and/or band ratios (Gad and Kusky, 2007; Inzana et al., 2003); 3) shape-fitting based algorithms such as Spectral Angle Mapper (SAM) (Kruse et al., 1993), Matched-Filtering (MF) (Boardman et al., 1995; Harsanyi et al., 1994), and Mixture-Tuned Matched-Filtering (MTMF) (Boardman, 1998; Boardman et al., 1995) which are a step above Principal Component Analysis (PCA), but a "partial unmixing" alternative below Linear Spectral Unmixing (LSU) (Adams et al., 1993; Boardman, 1993); and 4) Linear Spectral Unmixing (LSU) and similar methods such as Constrained Energy Minimization (CEM) (Boardman, 1989, 1992; Farrand and Harsanyi, 1994, 1997; Resmini et al., 1997). Table 1 lists summarized descriptions of the applied algorithms to ASTER data.

This review indicated that several image processing methods are applicable to ASTER data to detect hydrothermal alteration mineral zones associated with porphyry copper and epithermal gold mineralization and related host-rock lithology at both regional and district scales. Logical operator algorithms can be best suited for hydrothermal alteration mapping, including phyllic and argillic zones associated with copper/gold mineralization using ASTER data in a regional scale. The algorithms perform multiple band ratio and threshold value calculations, which can be applied to a scene of ASTER using a single algorithm, thus eliminating separate production and application of vegetation and dark pixel masks (Mars and Rowan, 2006). Some organic materials such as lignin-cellulose have spectral absorption features centered near 2.10 and 2.30 μm, which are near the distinctive absorption features of hydrothermal alteration minerals. The presence of organic materials has affected the remote detection of hydroxyl-bearing minerals (Mars and Rowan, 2006; Van Ruitenbeek et al., 2006). Thus, the elimination of vegetation is paramount in discriminating of hydrothermally altered rocks from surrounding area. Argillic and phyllic band-ratio logical operators use band ratios that define the 2.17 μm and 2.20 μm absorption features to map kaolinite and alunite, which are typical in argillic-altered rocks, and muscovite, which is a common mineral in phyllic-altered rocks (Mars and Rowan, 2006). Results extracted from the algorithms for detecting the spatial distribution of phyllic and argillic zones have good function in identifying hydrothermally altered mineral areas without any disturbances of vegetation effects.

Performing shape-fitting based and partial unmixing algorithms such as Spectral Angle Mapper, Matched-Filter, Mixture-Tuned Matched-Filtering, Linear Spectral Unmixing, and Constrained Energy Minimization is based on comparison of image reflectance spectra with library spectra of end-member minerals or reference spectra extracted directly from the image. Fortunately, as part of the ASTER activities, a library of over 2000 spectra of natural and man-made materials was compiled as the ASTER Spectral Library version 2.0 and made available from http://speclib.jpl.nasa.gov. The library includes spectra of rocks, minerals, lunar soils, terrestrial soils, manmade materials, meteorites, vegetation, snow and ice covering the visible through thermal infrared wavelength region (0.4–15.4 μm) (Baldridge et al., 2009). So, the spectra

Table 1
Descriptions of the algorithms applied to ASTER data.

Algorithm	Reference	Description
Principal Component Analysis (PCA)	Singh and Harrison (1985)	Principal Component Analysis (PCA) is a multivariate statistical technique that selects uncorrelated linear combinations (eigenvector loadings) of variables in such a way that each component successively extracted linear combination and has a smaller variance.
Minimum Noise Fraction (MNF)	Green et al.(1988); Boardman et al. (1995)	Minimum Noise Fraction (MNF) transformation is used to determine the inherent dimensionality of image data, segregate noise in the data, and reduce the computational requirements for subsequent processing.
Band ratio, Relative Absorption Band Depth (RBD), band indices, and logical operators	Rowan et al. (1977); Goetz et al. (1983); Sabins (1987); Crowley et al. (1989); Ninomiya (2003a, 2003b); Mars and Rowan (2006)	Band ratio is a technique where the digital number value of one band is divided by the digital number value of another band. Band ratios are very useful for highlighting certain features or materials that cannot be seen in the raw bands. Relative Absorption Band Depth (RBD) is a useful three-point ratio formulation for detecting diagnostic mineral absorption features. For each absorption feature, the numerator is the sum of the bands representing the shoulders, and the denominator is the band located nearest the absorption feature minimum. Band indices for ASTER VNIR, SWIR, and TIR have been explained in the text of this paper. Logical operator algorithm performs a series of band ratios for each pixel. Each logical operator determines a true or false value for each ratio by comparing the band ratio to a predetermined range of threshold values. All of the ratios in the algorithm have to be true in order for a value of 1 to be assigned to the byte image; otherwise a 0 value is produced. Thus, a byte image consisting of zeros and ones is produced with each algorithm.
Spectral Angle Mapper (SAM)	Kruse et al. (1993)	The Spectral Angle Mapper (SAM) technique measures the spectral similarity by calculating the angle between the two spectra and treating them as vectors in n-dimensional space.
Linear Spectral Unmixing (LSU)	Boardman (1993); Adams et al. (1993)	Linear Spectral Unmixing (LSU) is known as sub-pixel sampling, the reflectance at each pixel of the image is assumed to be a linear combination of the reflectance of each material (or end-member) present within the pixel.
Matched-Filtering (MF)	Harsanyi et al. (1994); Boardman et al. (1995)	The Matched-Filtering (MF) technique performs a partial unmixing of spectra to estimate the abundance of user-defined end-members from a set of reference spectra. This technique maximizes the response of the known end-member and suppresses the response of the composite unknown background, thus matching the known signature.
Mixture-Tuned Matched-Filtering (MTMF)	Boardman et al. (1995); Boardman (1998)	Mixture-Tuned Matched-Filtering (MTMF) technique is a combination of the Linear Spectral Unmixing technique and the statistical Matched Filtering model. From Matched Filtering it inherits the advantage of its ability to map a single known target without knowing the other background end-member signatures, unlike traditional Spectra Mixture modeling. From Spectral Mixture modeling it inherits the leverage arising from the mixed pixel model, the constraints on feasibility including the unit-sum and positivity requirements, unlike the Matched Filter which does not employ these fundamental facts. As a result MTMF can outperform either method, especially in cases of subtle, sub-pixel occurrences.
Constrained Energy Minimization (CEM)	Farrand and Harsanyi (1994, 1997); Resmini et al. (1997)	The Constrained Energy Minimization (CEM) technique is an implementation of matched filtering methods in the context of hyperspectral analysis. The CEM technique was developed by analogy to the solution of the typical adaptive beam-forming problem in the signal processing community. The CEM algorithm attempts to maximize the response of a target spectrum and suppress the response of the unknown background signature(s).

of selected end-member minerals can be taken from the ASTER Spectral Library version 2.0 for distinguishing hydrothermal alteration minerals. In addition, reference spectra can be extracted directly from ASTER image using AIG-Developed Hyperspectral Analysis methods which were developed by Kruse and Boardman (2000) and associates at Analytical Imaging and Geophysics LLC (AIG) for analyzing hyperspectral data. These approaches are implemented and documented within the "Environment for Visualizing Images" (ENVI) software system originally developed by AIG scientists (now an Eastman Kodak/Research Systems Inc. (RSI) commercial-off-the-shelf (COTS) product) (Kruse et al., 2003; Research Systems, Inc., 2001).

It is shown that the results derived from the shape-fitting based and partial unmixing algorithms are robust and reliable for detecting a particular mineral and mineral assemblages in hydrothermal alteration zones in a district scale. Consequently, the integration of the results derived from the logical operator, shape-fitting based, and partial unmixing algorithms can produce comprehensive and accurate information using ASTER data for the reconnaissance stages of copper and gold exploration at both regional and district scales.

4. Conclusions

This paper reviews performance characteristics of ASTER, the standard data products, and applications of the most recently developed image processing methods applied to the data as a tool for mapping hydrothermal alteration mineral zones associated with porphyry copper and epithermal gold mineralization and related host-rock lithology. The use of ASTER data in mineral exploration and lithological mapping has been increased in recent years due to: (i) spectral characteristics of the unique integral bands of ASTER, which are highly sensitive to hydrothermal alteration minerals especially in shortwave length infrared radiation region; (ii) the possibility of applying several image processing techniques; (iii) 'on-demand' data product availability with low cost (~$60 US or Yen equivalent); and (iv) broad 60 × 60 km scene coverage useful for regional scale mapping. It is this enhanced spectral resolution of ASTER in the SWIR wavelengths that allows for reconnaissance mineral exploration from a spaceborne platform.

Application of several image processing methods to ASTER data allows rapid extraction of useful information of interest such as alteration mineral types and abundances. Also, the availability and diversity of ASTER standard data products make them suitable remote sensing data for mineral exploration purposes. AST-07XT and RefL1b ASTER SWIR reflectance products can be used for mineral mapping projects without use of additional spectral data from the site for calibration. Especially, RefL1b data are more suitable for regional mineral mapping. Hydrothermal alteration zones associated with porphyry copper deposit such as phyllic, argillic, potassic, and propylitic can be discriminated from one another by virtue of spectral absorption features of their most dominant minerals, which are recognizable by ASTER SWIR special bands. Differentiation between phyllic, argillic, and propylitic zones can be critical as an indicator of highest mineralization potential, which is typically associated with phyllic alteration zones.

Four types of algorithms can be used to extract spectral information of ASTER data: (i) band-ratio, indices and logical operator based methods; (ii) principal components and enhancement based methods such as PCA and MNF; (iii) shape-fitting based algorithms such as SAM, MF, and MTMF; and (iv) partial unmixing methods such as LSU and CEM. Logical operator algorithms can be best suited for detecting of phyllic and argillic zones without any disturbances of vegetation effects in a regional scale. Shape-fitting based and partial unmixing techniques are robust and reliable for distinguishing specific mineral and mineral assemblages in hydrothermal alteration zones in a district scale. The integration of the logical operator, shape-fitting based, and partial unmixing algorithms can create comprehensive and precise information for the reconnaissance stages of copper/gold exploration. Accordingly, ASTER data can be best processed and analyzed to yield information about the spatial distribution of hydrothermal mineral alteration zones associated with porphyry copper and epithermal gold mineralization around the world, including those yet to be discovered.

Acknowledgments

This study was conducted as a part of the Fundamental Research Grant Scheme, Ministry of Higher Education Malaysia. We are grateful to the Universiti Teknologi Malaysia for providing the facilities for this investigation. We also thank reviewers for their comments, which were especially helpful in clarifying certain points in the manuscript.

References

Abdelsalam, M., Stern, R., 2000. Mapping gossans in arid regions with landsat TM and SIR-C images, the Beddaho Alteration Zone in northern Eritrea. J. Afr. Earth Sci. 30, 903–916.
Abrams, M., 2000. The Advanced Spaceborne Thermal Emission and Reflection Radiometer (ASTER): data products for the high spatial resolution imager on NASA's Terra platform. Int. J. Remote. Sens. 21, 847–859.
Abrams, M.J., Brown, D., 1984. Silver Bell, Arizona, porphyry copper test site report: Tulsa, Oklahoma. The American Association of Petroleum Geologists, the Joint NASA–Geosat Test Case Project, Final Report, Chapter 4, pp. 4–73.
Abrams, M., Hook, S.J., 1995. Simulated ASTER data for geologic studies. IEEE Trans. Geosci. Remote. Sens. 33 (3).
Abrams, M.J., Brown, D., Lepley, L., Sadowski, R., 1983. Remote sensing of porphyry copper deposits in Southern Arizona. Econ. Geol. 78, 591–604.
Abrams, M., Hook, S., Ramachandran, B., 2004. ASTER User Handbook, Version 2. Jet Propulsion Laboratory, California Institute of TechnologyOnline: http://asterweb.jpl.nasa.gov/content/03_data/04_Documents/aster_guide_v2.pdf2004.
Adams, J.B., Smith, M.O., Gillespie, A.R., 1993. Imaging spectroscopy: interpretation based on spectral mixture analysis. In: Pieters, C.M., Englert, P.A.J. (Eds.), Remote Geochemical Analysis: Elemental and Mineralogical Composition. Cambridge University Press, New York, pp. 145–166.
Baldridge, A.M., Hook, S.J., Grove, C.I., Rivera, G., 2009. The ASTER spectral library version 2.0. Remote Sens. Environ. 113, 711–715.
Bedell, R.L., 2001. Geological mapping with ASTER satellite: new global satellite data that is a significant leap in remote sensing geologic and alteration mapping. Special Publication Geology Society of Nevada, 33, pp. 329–334.
Bedini, E., Van Der Meer, F., Van Ruitenbeek, F., 2009. Use of HyMap imaging spectrometer data to map mineralogy in the Rodalquilar caldera, southeast Spain. Int. J. Remote. Sens. 30 (2), 327–348.
Biggar, S.F., Thome, K.J., McCorkel, J.T., D'Amico, J.M., 2005. Vicarious calibration of the ASTER SWIR sensor including crosstalk correction. Proc. Int. Soc. Opt. Eng. 5882, 588217.
Boardman, J.W., 1989. Inversion of imaging spectrometry data using singular value decomposition. IGARSS'89, 12th Canadian Symposium on Remote Sensing, pp. 2069–2072.
Boardman, J.W., 1992. Sedimentary facies analysis using imaging spectrometry: a geophysical inverse problem. Unpublished Ph.D. thesis, University of Colorado.
Boardman, J.W., 1993. Automated Spectral Unmixing of AVIRIS Data Using Convex Geometry Concepts: in Summaries, Fourth JPL Airborne Geoscience Workshop.
Boardman, J.W., 1998. Leveraging the high dimensionality of AVIRIS data for improved sub-pixel target unmixing and rejection of false positives: mixture tuned matched filtering. Summaries of the Seventh Annual JPL Airborne Geoscience Workshop, Pasadena, CA, p. 55.
Boardman, J.W., Kruse, F.A., Green, R.O., 1995. Mapping target signatures via partial unmixing of AVIRIS data, summaries. Proceedings of the Fifth JPL Airborne Earth Science Workshop, 23–26 January, Pasadena, California, JPL Publication 95–1, vol. 1, pp. 23–26.
Carranza, E.J., Hall, M., 2002. Mineral mapping with Landsat Thematic Mapper data for hydrothermal alteration mapping in heavily vegetated terrane. Int. J. Remote. Sens. 23 (22), 4827–4852.
Clark, R.N., King, T.V.V., Klejwa, M., Swayze, G.A., 1990. High spectral resolution reflectance spectroscopy of minerals. J. Geophys. Res. 95, 12653–12680.
Clark, R.N., Swayze, G.A., Gallagher, A., King, T.V.V., Calvin, W.M., 1993. . 1340 p. The U.S. Geological Survey, Digital Spectral Library: Version 1: 0.2 to 3.0 Microns: U.S. Geological Survey Open File Report 93–592http://speclab.cr.usgs.gov (August 1999).
Crosta, A.P., Filho, C.R.S., Azevedo, F., Brodie, C., 2003. Targeting key alteration minerals in epithermal deposits in Patagonia, Argentina, using ASTER imagery and principal component analysis. Int. J. Remote. Sens. 24, 4233–4240.
Crowley, J.K., Vergo, N., 1988. Near-infrared reflectance spectra of mixtures of kaolin group minerals: use in clay mineral studies. Clays Clay Miner. 36, 310–316.
Crowley, J.K., Brickey, D.W., Rowan, L.C., 1989. Airborne imaging spectrometer data of the Ruby Mountains, Montana: mineral discrimination using relative absorption band-depth images. Remote Sens. Environ. 29, 121–134.
Dalton, J.B., Bove, D.J., Mladinich, C.S., Rockwell, B.W., 2004. Identification of spectrally similar materials using the USGS Tetracorder algorithm: the calcite–epidot–chlorite problem. Remote Sens. Environ. 89, 455–466.

Di Tommaso, I., Rubinstein, N., 2007. Hydrothermal alteration mapping using ASTER data in the Infiernillo porphyry deposit, Argentina. Ore Geol. Rev. 32, 275–290.
Dilles, J.H., Einaudi, M.T., 1992. Wall-rock alteration and hydrothermal flow paths about the Ann-Mason porphyry copper deposit, Nevada-a 6-km vertical reconstruction. Econ. Geol. 87, 1963–2001.
Ducart, D.F., Crosta, A.P., Filio, C.R.S., 2006. Alteration mineralogy at the Cerro La Mina epithermal prospect, Patagonia, Argentina: field mapping, short-wave infrared spectroscopy, and ASTER images. Econ. Geol. 101, 981–996.
Farrand, W.H., Harsanyi, J.C., 1994. Mapping distributed geological and botanical targets through constrained energy minimization. Proceedings, 10th Thematic Conference on Geological Remote Sensing, San Antonio, TX, 9–12 May 1994, pp. I-419–I-429.
Farrand, W.H., Harsanyi, J.C., 1997. Mapping the distribution of mine tailings in the Coeur d'Alene River Valley, Idaho, through the use of a constrained energy minimization technique. Remote Sens. Environ. 59 (1), 64–76.
Ferrier, G., Wadge, G., 1996. Application of imaging spectrometry data to mapping alteration zones associated with gold mineralization in southern Spain. Int. J. Remote. Sens. 17, 331–350.
Ferrier, G., White, K., Griffiths, G., Bryant, R., Stefouli, M., 2002. The mapping of hydrothermal alteration zones on the island of Lesvos, Greece, using an integrated remote sensing data set. Int. J. Remote. Sens. 23, 341–356.
Fujisada, H., 1995. Design and performance of ASTER instrument. In: Breckinridge, J.B. (Ed.), Proceedings of International Society of Optical Engineering, 2583, pp. 16–25.
Gabr, S., Ghulam, A., Kusky, T., 2010. Detecting areas of high-potential gold mineralization using ASTER data. Ore Geol. Rev. 38, 59–69.
Gad, S., Kusky, T., 2007. ASTER spectral ratioing for lithological mapping in the Arabian–Nubian shield, the Neoproterozoic Wadi Kid area, Sinai, Egypt. Gondwana Res. 11, 326–335.
Galvao, L.S., Filho, R.A., Vitorello, I., 2005. Spectral discrimination of hydrothermally altered materials using ASTER short-wave infrared bands: evaluation in a tropical savannah environment. Int. J. Appl. Earth Obs. Geoinf. 7, 107–114.
Gillespie, A.R., Matsunaga, T., Rokugawa, S., Hook, S.J., 1998. Temperature and emissivity separation from Advanced Spaceborne Thermal Emission and Reflection Radiometer (ASTER) images. IEEE Trans. Geosci. Remote. Sens. 36, 1113–1126.
Gillespie, A., Abrams, M., Yamaguchi, Y., 2005. Scientific results from ASTER. Remote Sens. Environ. 99, 1.
Goetz, A.F.H., Rock, B.N., Rowan, L.C., 1983. Remote sensing for exploration: an overview. Econ. Geol. 78, 573–590.
Green, A.A., Berman, M., Switzer, P., Craig, M.D., 1988. A transformation for ordering multispectral data in terms of image quality with implications for noise removal. IEEE Trans. Geosci. Remote Sens. 26 (1), 65–74.
Harsanyi, J.C., Farrand, W.H., Chang, C.I., 1994. Detection of subpixel signatures in hyperspectral image sequences. Proceedings of 1994 ASPRS Annual Conference, Reno, Nevada, pp. 236–247.
Hewson, R.D., Cudahy, T.J., Mizuhiko, S., Ueda, K., Mauger, A.J., 2005. Seamless geological map generation using ASTER in the Broken Hill–Curnamona province of Australia. Remote Sens. Environ. 99, 159–172.
Hunt, G.R., 1977. Spectral signatures of particulate minerals in the visible and near infrared. Geophysics 42, 501–513.
Hunt, G.R., Ashley, P., 1979. Spectra of altered rocks in the visible and near infrared. Econ. Geol. 74, 1613–1629.
Hunt, G.R., Salisbury, J.W., 1974. Mid-infrared spectral behavior of igneous rocks. Technical report AFRCL-TR-75-0356. US Air Force Cambridge Research Laboratory, Cambridge, MA.
Huntington, J.F., 1996. The role of remote sensing in finding hydrothermal mineral deposits on Earth. Evolution of Hydrothermal Ecosystems on Earth (and Mars?). Wiley, England, pp. 214–234.
Inzana, J., Kusky, T., Higgs, G., Tucker, R., 2003. Supervised classifications of Landsat TM band ratio images and Landsat TM band ratio image with radar for geological interpretations of central Madagascar. J. Afr. Earth Sci. 37, 59–72.
Iwasaki, A., Tonooka, H., 2005. Validation of a crosstalk correction algorithm for ASTER/SWIR. IEEE Trans. Geosci. Remote. Sens. 43, 2747–2751.
Kanlinowski, A., Oliver, S., 2004. ASTER mineral index processing. Remote Sensing Application Geoscience Australia. Australian Government Geoscience. Website: http://www.ga.gov.au/image_cache/GA7833.pdf.
Kratt, C., Calvin, W.M., Coolbaugh, M.F., 2010. Mineral mapping in the Pyramid Lake basin: hydrothermal alteration, chemical precipitates and geothermal energy potential. Remote Sens. Environ. 114 (10), 2297–2304.
Kruse, F.A., Boardman, J.W., 2000. Characterization and mapping of kimberlites and related diatremes using hyperspectral remote sensing. Proceeding. 2000 IEEE Aero-Space Conference., Big Sky, MO, March 18–24.
Kruse, F.A., Boardman, J.W., Lefkoff, A.B., Heidebrecht, K.B., Shapiro, A.T., Barloon, P.J., Goetz, A.F.H., 1993. The Spectral Image Processing System (SIPS) — interactive visualization and analysis of imaging spectrometer data. Remote Sens. Environ. 44, 145–163.
Kruse, F.A., Bordman, J.W., Huntington, J.F., 2003. Comparison of airborne hyperspectral data and EO-1 Hyperion for mineral mapping. IEEE Trans. Geosci. Remote Sens. 41 (6), 1388–1400.
Lowell, J.D., Guilbert, J.M., 1970. Lateral and vertical alteration–mineralization zoning in porphyry ore deposits. Econ. Geol. 65, 373–408.
Mars, J.C., Rowan, L.C., 2006. Regional mapping of phyllic- and argillic-altered rocks in the Zagros magmatic arc, Iran, using Advanced Spaceborne Thermal Emission and Reflection Radiometer (ASTER) data and logical operator algorithms. Geosphere 2, 161–186.
Mars, J.C., Rowan, L.C., 2010. Spectral assessment of new ASTER SWIR surface reflectance data products for spectroscopic mapping of rocks and minerals. Remote Sens. Environ. 114, 2011–2025.
Moghtaderi, A., Moore, F., Mohammadzadeh, A., 2007. The application of advanced space-borne thermal emission and reflection (ASTER) radiometer data in the detection of alteration in the Chadormalu paleocrater, Bafq region, Central Iran. J. Asian Earth Sci. 30, 238–252.
Moore, F., Rastmanesh, F., Asady, H., Modabberi, S., 2008. Mapping mineralogical alteration using principal component analysis and matched filter processing in Takab area, north-west Iran, from ASTER data. Int. J. Remote. Sens. 29, 2851–2867.
Ninomiya, Y., 2003a. A stabilized vegetation index and several mineralogic indices defined for ASTER VNIR and SWIR data. Proc. IEEE 2003 International Geoscience and Remote Sensing Symposium (IGARSS'03) Vol. 3, Toulouse, France, 21–25 July 2003, pp. 1552–1554.
Ninomiya, Y., 2003b. Advanced remote lithologic mapping in ophiolite zone with ASTER multispectral thermal infrared data. Proc. IEEE 2003 International Geoscience and Remote Sensing Symposium (IGARSS'03) Vol. 3, Toulouse, France, 21–25 July 2003, pp. 1561–1563.
Ninomiya, Y., 2003c. Rock type mapping with indices defined for multispectral thermal infrared ASTER data: case studies. Proc. SPIE 4886, 123–132.
Ninomiya, Y., 2004. Lithological mapping with ASTER TIR and SWIR data. Proc. SPIE 5234, 180–190.
Ninomiya, Y., Fu, B., 2002. Mapping quartz, carbonate minerals and mafic–ultramafic rocks using remotely sensed multispectral thermal infrared ASTER data. Proc. SPIE 4710, 191–202.
Ninomiya, Y., Fu, B., Cudahy, T.J., 2005. Detecting lithology with Advanced Spaceborne Thermal Emission and Reflection Radiometer (ASTER) multispectral thermal infrared "radiance-at-sensor" data. Remote Sens. Environ. 99 (1–2), 127–139.
Perry, S.L., 2004. Spaceborne and airborne remote sensing systems for mineral exploration–case histories using infrared spectroscopy. In: King, P.L., Ramsey, M.S., Swayze, G.A. (Eds.), Infrared Spectroscopy in Geochemistry, Exploration Geochemistry, and Remote Sensing. Mineralogical Association of Canada, London, Canada, pp. 227–240.
Pieri, D., Abrams, M., 2004. ASTER watches the world's volcanoes: a new paradigm for volcanological observations from orbit. J. Volcanol. Geotherm. Res. 135, 13–28.
Pour, B.A., Hashim, M., 2011. Spectral transformation of ASTER data and the discrimination of hydrothermal alteration minerals in a semi-arid region, SE Iran. Int. J. Phys. Sci. 6 (8), 2037–2059.
Pour, B.A., Hashim, M., Marghany, M., 2011. Using spectral mapping techniques on short wave infrared bands of ASTER remote sensing data for alteration mineral mapping in SE Iran. Int. J. Phys. Sci. 6 (4), 917–929.
Research Systems, Inc., 2001. ENVI Tutorials. Research Systems, Inc, Boulder, CO.
Resmini, R.G., Kappus, M.E., Aldrich, W.S., Harsanyi, J.C., Anderson, M., 1997. Mineral mapping with hyperspectral digital imagery collection experiment (HYDICE) sensor data at Cuprite, Nevada, USA. Int. J. Remote. Sens. 18 (7), 1553–1570.
Rockwell, B.W., Hofstra, A.H., 2008. Identification of quartz and carbonate minerals across northern Nevada using ASTER thermal infrared emissivity data implications for geologic mapping and mineral resource investigations in well-studied and frontier areas. Geosphere 4 (1), 218–246.
Rowan, L.C., Goetz, A.F.H., Ashley, R.P., 1977. Discrimination of hydrothermally altered and unaltered rocks in visible and near infrared multispectral images. Geophysics 42 (3), 522–535.
Rowan, L.C., Hook, S.J., Abrams, M.J., Mars, J.C., 2003. Mapping hydrothermally altered rocks at Cuprite, Nevada, using the Advanced Spaceborne Thermal Emission and Reflection Radiometer (ASTER), a new satellite-imaging system. Econ. Geol. 98 (5), 1019–1027.
Rowan, L.C., Mars, J.C., Simpson, C.J., 2005. Lithologic mapping of the Mordor N.T, Australia ultramafic complex by using the Advanced Spaceborne Thermal Emission and Reflection Radiometer (ASTER). Remote Sens. Environ. 99, 105–126.
Rowan, L.C., Schmidt, R.G., Mars, J.C., 2006. Distribution of hydrothermally altered rocks in the Reko Diq, Pakistan mineralized area based on spectral analysis of ASTER data. Remote Sens. Environ. 104, 74–87.
Sabins, F.F., 1987. Remote Sensing Principles and Interpretation, 2nd edition. Freeman, New York.
Sabins, F.F., 1999. Remote sensing for mineral exploration. Ore Geol. Rev. 14, 157–183.
Sillitoe, R.H., 2010. Porphyry copper systems. Econ. Geol. 105, 3–41.
Singh, A., Harrison, A., 1985. Standardized principal components. Int. J. Remote. Sens. 6, 883–896.
Spatz, D.M., Wilson, R.T., 1995. Remote sensing characteristics of porphyry copper systems, western America Cordillera. In: Pierce, F.W., Bolm, J.G. (Eds.), Arizona Geological Society Digest, 20, pp. 94–108.
Tangestani, M.H., Moore, F., 2002. Porphyry copper alteration mapping at the Meiduk area, Iran. Int. J. Remote. Sens. 23 (22), 4815–4825.
Tangestani, M.H., Mazhari, N., Ager, B., Moore, F., 2008. Evaluating advance spaceborne thermal emission and reflection radiometer (ASTER) data for alteration zone enhancement in a semi-arid area, northern Shahr-e-Babak, SE Iran. Int. J. Remote. Sens. 29 (10), 2833–2850.
Thome, K., Palluconi, F., Takashima, T., Masuda, K., 1998. Atmospheric correction of ASTER. IEEE Trans. Geosci. Remote Sens. 36 (4), 1119–1211.
Van Ruitenbeek, F.J.A., Pravesh, D., Van Der Meer, F.D., Cudahy, T., Van Der Meijde, M., Hale, M., 2006. Mapping white micas and their absorption wavelengths using hyperspectral band ratios. Remote Sens. Environ. 102, 211–222.
Velosky, J.C., Stern, R.J., Johnson, P.R., 2003. Geological control of massive sulfide mineralization in the Neoproterozoic Wadi Bidah shear zone, southwestern Saudi Arabia, inferences from orbital remote sensing and field studies. Precambrian Res. 123 (2–4), 235–247.
Xu, Y., Qizhong, L., Yun, S., Lu, W., 2004. Extraction mechanism of alteration zones using ASTER imagery. Geosciences and Remote Sensing Symposium, IGARSS 04, Proceeding 2004 IEEE International, 6, pp. 4174–4175.

Yamaguchi, Y., Naito, C., 2003. Spectral indices for lithologic discrimination and mapping by using the ASTER SWIR bands. Int. J. Remote. Sens. 24 (22), 4311–4323.
Yamaguchi, Y.I., Fujisada, H., Kudoh, M., Kawakami, T., Tsu, H., Kahle, A.B., Pniel, M., 1999. ASTER instrument characterization and operation scenario. Adv. Space Res. 23 (8), 1415–1424.
Yamaguchi, Y.I., Fujisada, H., Kahle, A.B., Tsu, H., Kato, M., Watanabe, H., Sato, I., Kudoh, M., 2001. ASTER instrument performance, operation status, and application to Earth sciences. IEEE Transactions of Geosciences and Remote Sensing, pp. 1215–1216.
Yujun, Z., Jianmin, Y., Fojun, Y., 2007. The potentials of multi-spectral remote sensing techniques for mineral prognostication — taking Mongolian Oyu Tolgoi Cu–Au deposit as an example. Earth Sci. Front. 14 (5), 63–70.
Zhang, X., Panzer, M., Duke, N., 2007. Lithologic and mineral information extraction for gold exploration using ASTER data in the south Chocolate Mountains (California). J. Photogramm. Remote Sens. 62, 271–282.